Supplementary Information

Coacervate-based Underwater Adhesives in Physiological Conditions

Mehdi Vahdati, Francisco J. Cedano-Serrano, Costantino Creton*, Dominique Hourdet*

Soft Matter Sciences and Engineering, ESPCI Paris, PSL University, Sorbonne University, CNRS, F-75005 Paris, France

costantino.creton@espci.fr, dominique.hourdet@espci.fr

Synthesis of the polyelectrolytes.

We followed a simple procedure previously reported by our group for neutral monomers.[1,2] In this method based on free radical polymerization, a chain transfer agent used as a redox co-initiator allows to control the molecular weight. For PMADAP telomer, 1 mmol (~ 17 g) of MADAP was first dissolved in MilliQ water in a 3-necked flask. The flask was then sealed and the solution was bubbled with N_2 gas for 1 h before the start of the reaction. 1 mmol of KPS and 2 mmol of AET-HCl were separately dissolved in MilliQ water and bubbled with nitrogen for 1 h. Next, the initiators were injected into the 3-necked flask in a dropwise manner and the reaction was allowed to proceed to overnight. In the end, an excess of NaOH was added into the solution to neutralize the HCl and recover the PMADAP in the basic form. The reaction medium was freeze-dried without further purification. Note that the excess sodium ions will be removed during dialysis after the next step.

The dry telomer (1 mmol of MADAP) was dissolved in 120 ml of NMP after 1 h of heating (60 °C) and vigorous stirring. Separately, 20 mmol of AA and 10 mmol of the coupling agent (DCCI) were dissolved in 15 ml of NMP. Note that both AA and DCCI are in large excess to the

initial AET concentration used in the first step. The AA solution was mixed with the telomer solution that was allowed to homogenize. DCCI was then added to start the reaction which proceeded overnight. The macromonomer solution was then diluted 2 times with water and purified by dialysis (membrane cut-off 3.5 kg.mol^{-1}) against MilliQ water changed twice per day for 1 week, such that the macromonomer was thus obtained in the protonated form.

From the ^{1}H-NMR spectrum presented in **Figure S1**, the polymer was found to have a number average molecular weight of 17000 g.mol^{-1} corresponding to an average DP of 100. For this analysis, we calculated the ratio between the dimethyl hydrogens of MADAP units (marked as a, appearing at 2.28 ppm) with those on the terminal double bond (marked as g and h, appearing at 5.6-6.2 ppm).

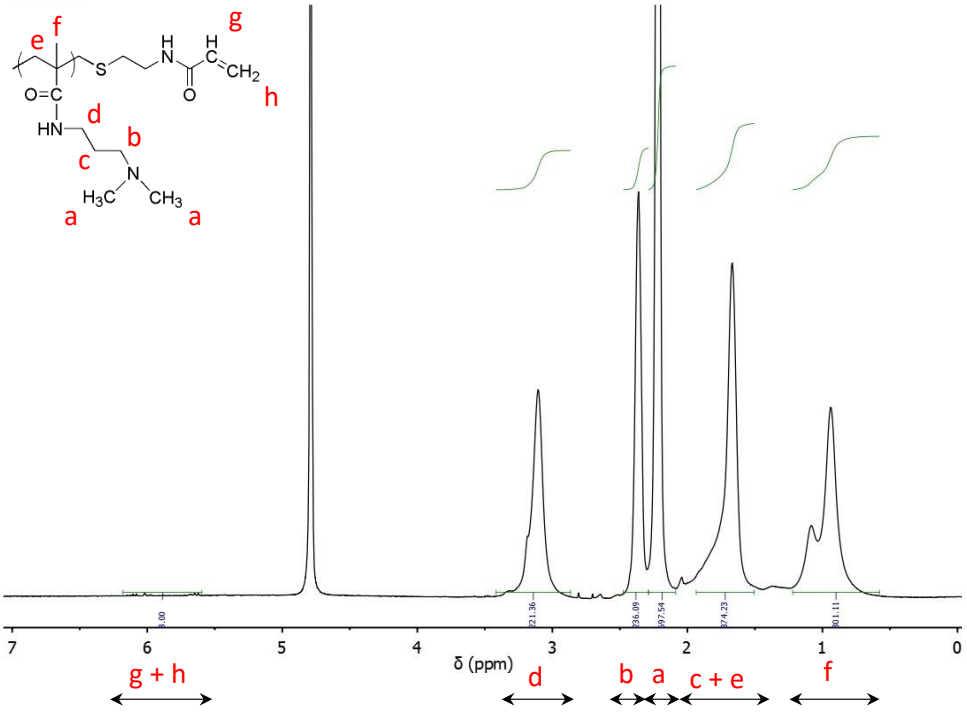

Figure S1. *^{1}H-NMR spectrum of PMADAP terminated with a double bond. Peak assignment is done using letters in red.*

PAMPS was synthesized similarly, but the terminal double bond was introduced using a water-mediated coupling reaction using EDC/NHS because AMPS is insoluble in most convenient organic solvents, including NMP.[3] Using ^{1}H-NMR, the polymer was found to have a number average molecular weight of 14000 kg.mol^{-1} (corresponding to an average DP of 70).

TGA: validation.

Before presenting TGA results from the coacervates, we first validate the hypotheses we have made. **Figure S2** plots weight losses from a 1M NaCl solution and an aqueous solution containing 8 wt % of a copolymer (PNIPAM-g-PAMPS) which is 64 wt % composed of AMPS units. In the case of the former sample, the TGA curve confirms complete removal of NaCl by 1000 °C starting around 800 °C. With the copolymer, the weight remains constant above 650 °C. We have therefore taken 700 °C as the border between changes in weight due to polymer and salt.

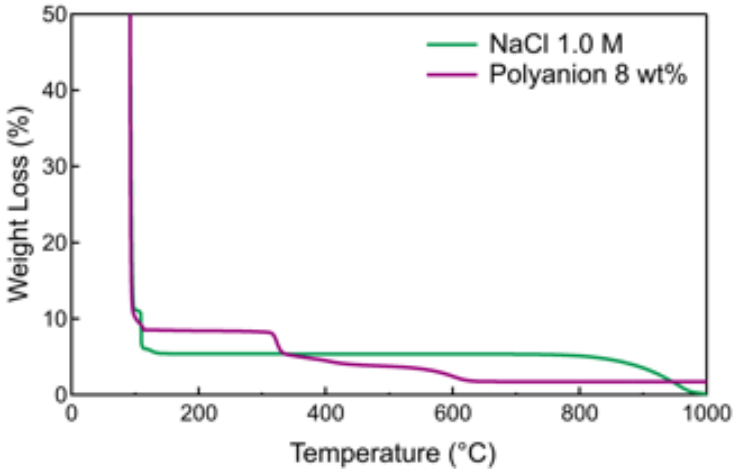

Figure S2. *Weight loss from a solution of NaCl (1.0 M) and a polyanion copolymer solution (8 wt %) containing 64 wt% PAMPS. The residual weight at 1000 °C corresponds to 32 wt % of PAMPS.*

The plateau at 650 °C can be assigned to the highly stable SO_3^- moiety. As we will see with the TGA graphs of the coacervates, this residual weight complicates distinguishing the polymer content in the coacervates. On the other hand, the salt concentration in the supernatant is measured with high accuracy due to its negligible polymer content (between 0.1 and 0.6 wt %). Assuming equal salt concentrations in both phases then allows a reasonable estimation of the polymer weight fraction in the coacervate phase, as shown in the following part.

TGA: composition calculations.

Figure S3 presents TGA curves for the coacervate and supernatant phases of the 0.5 M sample, as an example (note that the *y* axis only extends to 50 % of the total weight loss for higher magnification). The supernatant is mainly composed of water (97.05 wt %) and salt (2.83 wt %), with negligible polymer content (0.12 wt %). The TGA data of the coacervates suggests somewhat higher salt concentrations in this phase, but we have assumed the equal salt contents in both phases (2.83 wt % salt in the coacervate, as explained above. This gives a polymer content of 40.25 wt % in the coacervate, which contains 56.9 wt % water. Raw TGA data was obtained similarly for all the coacervates. For the salty polyelectrolyte solution above the CSC, the data corresponds to the single phase obtained.

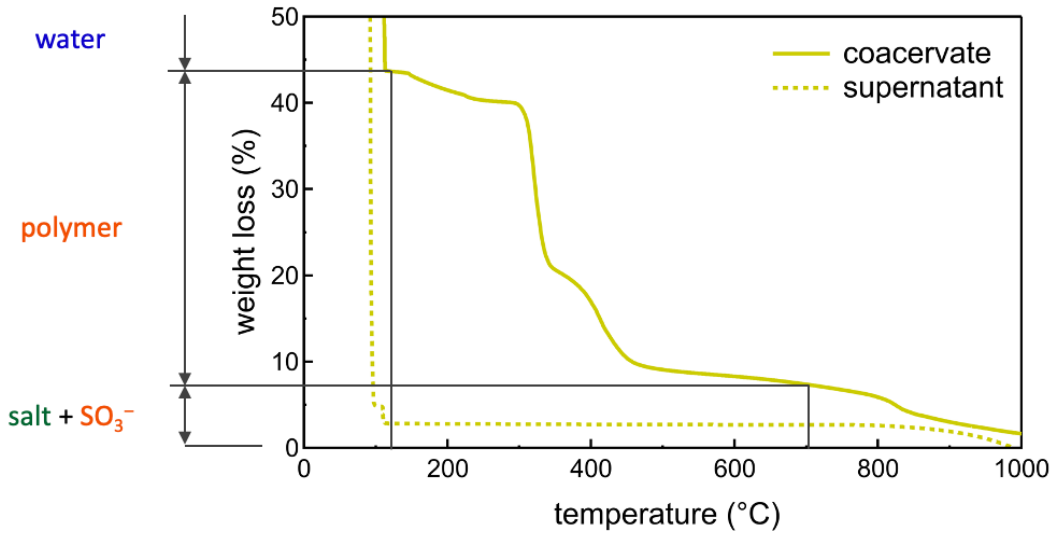

Figure S3. *Weight loss from the 0.5 M coacervate (solid line) and supernatant (dotted line). The raw data extracted for the coacervate phase is given beside the graph.*

For each sample, we first calculate the mass of the two phases (m_{CC} and m_{SN}) based on the polymer weight fraction in that phase ($w_{P,\varphi}$ where index φ denotes either CC or SN), the total weight of polymer in the sample ($m_{P,total} = 0.247\ g$) and the total mass of each sample (m_{total}) by writing:

$$w_{P,CC}m_{CC} + w_{P,SN}m_{SN} = m_{P,total} \tag{S1}$$

and

$$m_{CC} + m_{SN} = m_{total} \tag{S2}$$

We assume equal densities in both phases based on the corresponding salt solution; e.g. the 0.5 M sample with a density of ρ = 1.019 g.cm^{-3}, corresponding to that of a 0.5 M NaCl solution, weighs 14.27 g. The density is then used to work out the volume of each phase, which is necessary for molar concentrations. For instance, in the case of the 0.5 M homopolymer complex coacervate:

$$0.4025 \times m_{CC} + 0.0012 \times m_{SN} = 0.247$$

$$m_{CC} + m_{SN} = 14.27$$

$$\Rightarrow m_{CC} = 0.57\ g, m_{SN} = 13.70\ g$$

$$\Rightarrow V_{CC} = 0.56\ g, V_{SN} = 13.44\ g$$

The polymer weight fraction in each phase ($w_{P,\varphi}$) can be turned into its mass ($m_{P,\varphi}$) and moles ($n_{P,\varphi}$) by writing:

$$m_{P,\varphi} = w_{P,\varphi} V_{\varphi} \rho \tag{S3}$$

and

$$n_{P,\varphi} = m_{P,\varphi} \sum \frac{x_i}{M_i} \tag{S4}$$

In equation S4, *x* and *M* are, respectively, the molar mass of each comonomer (*i*) and its mass fraction in the total sample (SN + CC) according to the preparation formulation. We assume this ratio in both phases remains equal to that at preparation. The molarity of the polymer ($C_{P,\varphi}$) is then given as:

$$C_{P,\varphi} = n_{P,\varphi}/V_{\varphi} = w_{P,\varphi} \rho_{\varphi} \sum \frac{x_i}{M_i} \tag{S5}$$

These equations are similarly written for water (W) and salt (S).

For instance, in the case of the CC phase of the 0.5 M sample, we wrote

$$m_{P,CC} = 0.4025 \times 0.56(ml) \times 1.019(g.cm^{-3}) = 0.23\ g$$

$$n_{P,CC} = 0.23(g) \times \left\{\frac{0.483}{170.25} + \frac{0.517}{207.24}\right\}(mol.g^{-1}) = 1.23 \times 10^{-3}\ mol$$

$$C_{P,\varphi} = 1.23 \times 10^{-3}(mol)/0.56(ml) \times 10^{-3}(L) = 2.19\ mol.L^{-1}$$

The moles of salt were obtained similarly:

$$m_{S,CC} = 0.0283 \times 0.56(ml) \times 1.019(g.cm^{-3}) = 0.02\ g$$

$$n_{S,CC} = 0.02(g)/58.44(g.mol^{-1}) = 0.28 \times 10^{-3}\ mol$$

Calculations based on equilibrium.

Breaking macroion pairs PE^+PE^- into charges compensated by counter ions is governed by the following equilibrium:

$$PE^+PE^- + Na^+ + Cl^- \leftrightarrows PE^+Cl^- + PE^-Na^+ \quad \text{(S6)}$$

The equilibrium constant between paired and unpaired polyelectrolytes, *K*, may be written as follows:

$$K = \frac{[PE^+Cl^-][PE^-Na^+]}{[PE^+PE^-][Na^+][Cl^-]} = \frac{[PE^+Cl^-][PE^-Na^+]}{[PE^+PE^-][NaCl]^2} = \frac{y^2[PE]}{(1-y)[NaCl]^2} \quad \text{(S7)}$$

with $[PE^+Cl^-] = [PE^-Na^+] = y[PE]$ and $[PE^+PE^-] = (1-y)[PE]$. Therefore:

$$K[NaCl] = \frac{1}{r}\frac{y^2}{(1-y)} \quad \text{(S8)}$$

Using equation S8 at low salt concentration, where most added counter ions form ion pairs with polyelectrolyte counterparts ($y \cong r \ll 1$), it is possible to determine the proportionality constant which is simply the constant K of the dissociation equilibrium :

$$K[NaCl] = y \quad \text{(S9)}$$

Similarly using equations S7 and S9 we get :

$$K[PE] = (1-y) \quad \text{(S10)}$$

Then, the doping level can be extrapolated from the experimental salt to polymer ratio, *r*, in the coacervate using equations S9 and S10:

$$r = \frac{[NaCl]}{[PE]} = \frac{y}{(1-y)} \quad \text{(S11)}$$

Which is the same as equation 8 in the main text.

Table S1 presents nominal and experimentally measured concentrations of salt in the samples. The molar concentration of polyelectrolytes in the coacervate phase, $[PE^+] + [PE^-]$, is also given. Note that the polymer concentration in the total volume of each sample

is 0.094 M. This allows the calculation of the ratio between salt and polyelectrolytes in the coacervate phase, r, and the doping level, y, as defined by equations (6) and (8) in the main text and plotted in **Figure 5**.

Table S1. *Real salt ($[NaCl]$) concentration in the total volume of the samples at each nominal salt concentration, total polyelectrolyte ($[PE^+] + [PE^-]$) concentration in the coacervate phase, and the parameters* $r = \frac{[Na^+]+[Cl^-]}{[PE^+]+[PE^-]}$ *and* $y = \frac{r}{1+r}$.

$[NaCl]_{nominal}$	$[NaCl]$	$[PE^+] + [PE^-]$	r	y
0.0 M	≈ 0.0 M	1.77	0.038	0.037
0.1 M	0.11 M	2.33	0.093	0.085
0.5 M	0.49 M	2.18	0.451	0.311
0.75 M	0.73 M	1.86	0.784	0.439
1.0 M	1.07 M	0.79	2.714	0.731
1.2 M	1.14 M	0.58	3.921	0.797

Swelling in terms of relative volumes.

The stacked bar chart in **Figure S4** shows the relative volume of each phase, CC and SN, in the total volume of the complex coacervate as a function of the nominal salt concentration. Therefore, $\phi_{\mathrm{rel,CC}} = V_{CC}/14\mathrm{ml} \times 100$. Apart from the salt-free sample, the water content in the coacervate (swelling) increases with salt concentration. This trend is consistent with the pictures of the samples shown in **Figure 2** in the main text. As explained before, the volume of the sample prepared with no added salt is slightly larger than that of 0.1 M due to the chains that are in a kinetically-trapped state and have locally charged segments. This increases the water content compared to a sample with faster dynamics due to added salt (the 0.1 M sample).[4]

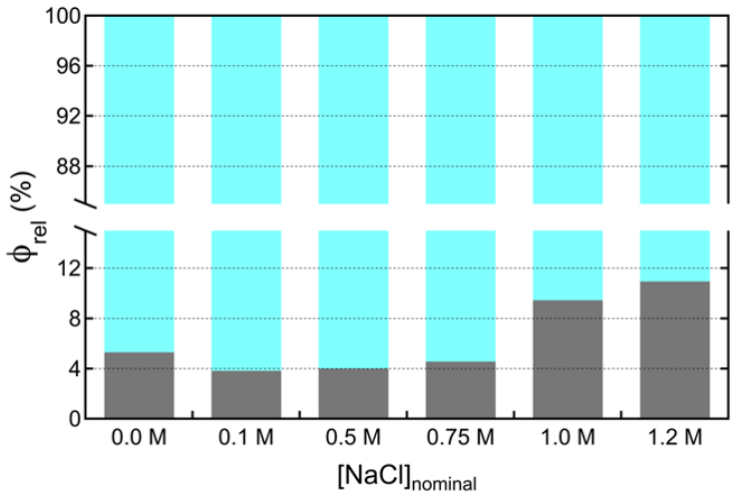

Figure S4. *Swelling expressed in terms of the relative volume (ϕ_{rel}) of each phase to the total volume at different nominal salt concentrations. The coacervate and supernatant phases are represented by gray and blue, respectively. Note that the sum of the two equals 100 vol %.*

TSS calculations.

The frequency-dependence of the complex viscosity of the samples prepared at 0.1 – 1.2 M NaCl is plotted in **Figure S5 A**. The low-frequency range of the more fluid-like samples was removed due to lack of accuracy, but the zero shear viscosity (η_0) is clear from the data points presented. The other samples show a marked shear-thinning behavior, typical of viscoelastic fluid samples like polymer solutions. As it can be seen, η_0 changes by more than 4 decades as a function of salt concentration.

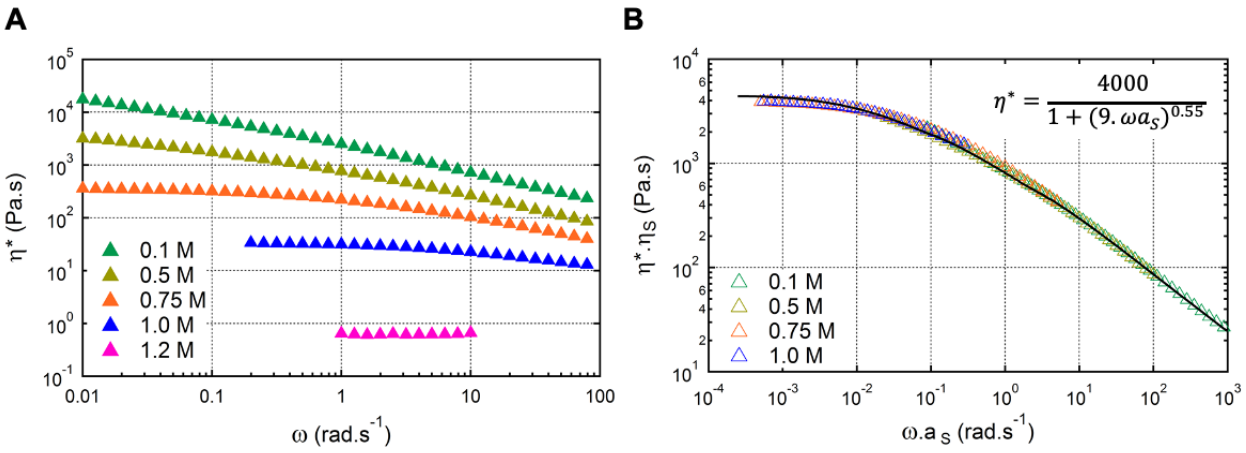

Figure S5. A. *Plots of complex viscosity versus angular frequency for coacervates prepared at different salt concentrations. Low-frequency data points without sufficient accuracy have been removed.* ***B.*** *Complex viscosity master curve obtained from the application of Time Salt Superposition. The solid line is the fit to the Cross model (equation shown).*

In order to calculate the shift factors for TSS, we fitted the shear-thinning behavior of the complex coacervates with Cross model.[5,6]

$$\eta^* = \eta_\infty + \frac{\eta_0 - \eta_\infty}{1+(\tau\omega)^n} \quad \text{(S12)}$$

Where η_0 and η_∞ are the viscosity at very low and very high frequencies, respectively. τ is the (longest) relaxation time of the system and *n* is an exponent obtained from the best fit to the data. Given that $\eta_\infty \ll \eta_0$ in this case (**Figure S5 A**), equation S12 can be written as:

$$\eta^* = \frac{\eta_0}{1+(\tau\omega)^n} \quad \text{(S13)}$$

By appropriate choice of η_0 from the raw data at low frequency, we fitted the curves in **Figure S5 A** with equation S13 using the same exponent (n= 0.55) and determined the relaxation times τ. Having τ and η_0, we then calculated the corresponding shear modulus (G) as:

$$G \cong \frac{\eta_0}{\tau} \quad \text{(S14)}$$

The shift factors presented in **Figure 8 B** in the main text were then calculated by taking the 0.5 M sample as the reference as:

$$a_S = \frac{\tau^s}{\tau^{ref}} \quad \text{(S15)}$$

and

$$b_S = \frac{G^s}{G^{ref}} \quad \text{(S16)}$$

In equation S15 and S16, the superscripts *ref* and *s* denote the reference and the sample for which the shift factor is calculated. The fact that the vertical shift factor (b_S) is not affected by the pre-factor in the calculation of G is evident from equation S15 (the ratio of two moduli with the same pre-factor).

Similarly, using a vertical shift factor ($\eta_S = 1/(a_s.b_s)$, the ratio of the zero shear viscosities of the reference and the sample under question) and the frequency shift factor a_S, we superimposed the viscosity data. In this way, the master curve and the equation given in **Figure S5 B** allow covering more than 5 decades of frequency.

Salt switch via linear rheology.

For the coacervates studied as model underwater adhesives, we probed the evolution of the dynamic moduli upon immersion in a medium resembling physiological conditions (0.1 M NaCl solution, pH = 7), as shown in **Figure S6**. For the sample containing a considerably higher salt concentration than the medium, there is an initial jump in the moduli (~ 1 h) followed by a long-lived pseudo-plateau where they stay close in value. The approach towards a critical gel point signals formation of extra macro-ion pairs due to ejection of salt into the medium. Although a crossover in the moduli takes ~ 8 h to realize, the main gain in properties occurs in the 1st hour (when the probe tack experiments were performed). Clearly, salt switch is a slow, diffusion-

controlled process which is kinetically more favorable through a less viscous coacervate (the diffusion coefficient of a simple spherical particle in a liquid is inversely proportional to its viscosity).[7]

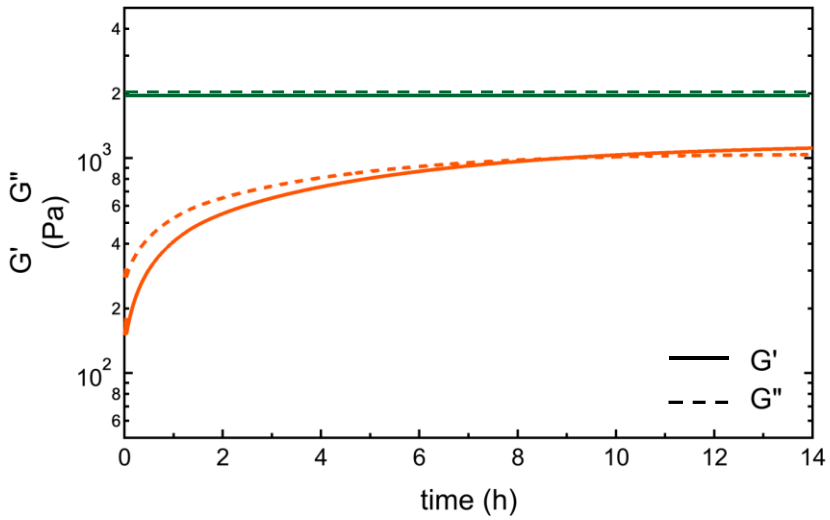

Figure S6. *Time sweep experiments immediately after immersion of 0.1 M (in green) and 0.75 M (in orange) coacervates in a 0.1 M NaCl solution at pH = 7.*

On the other hand, the sample already prepared at physiological conditions shows no change in mechanical properties, which indicates no major salt switch occurs in this case. This was expected given that the salt concentration is already equilibrated in NaCl 0.1 M. More interestingly, the 0.75 M sample does not eventually reach the same final mechanical properties as the sample prepared at 0.1 M after having been left in the same medium to reach equilibrium. This is because, even though they contain similar amounts of salt after the switch, their polymer concentration remains unchanged with roughly 10 wt % less polymer in the 0.75 M coacervate. A less likely, but plausible reason for this might be the shrinkage of the sample and a weaker interface with the

probes, although we believe this to be less likely as no macroscopic volume change was visually observed.

The above findings further highlight the necessity of considering the role of all the components in these soft materials, especially because the current literature places most of its focus on the salt concentration, overlooking the significance of water and polymer content.

Direct contact underwater.

Figure S7 shows the results of probe tack experiments on the 0.1 M coacervate after contact was directly established under water. For this, the chamber was filled with 0.1 M NaCl solution. An appropriate volume of the 0.1 M sample was taken with a spatula and placed on the glass slide. The probe came directly into contact with the coacervate which was squeezed to the intended initial thickness followed by 1 h of waiting time. The probe was then pulled at 0.2 s^{-1}. The nominal stress-strain curve and the adhesion energy are similar to those from underwater measurements after contact in air (for a typical curve, see **Figure 9** in the main text).

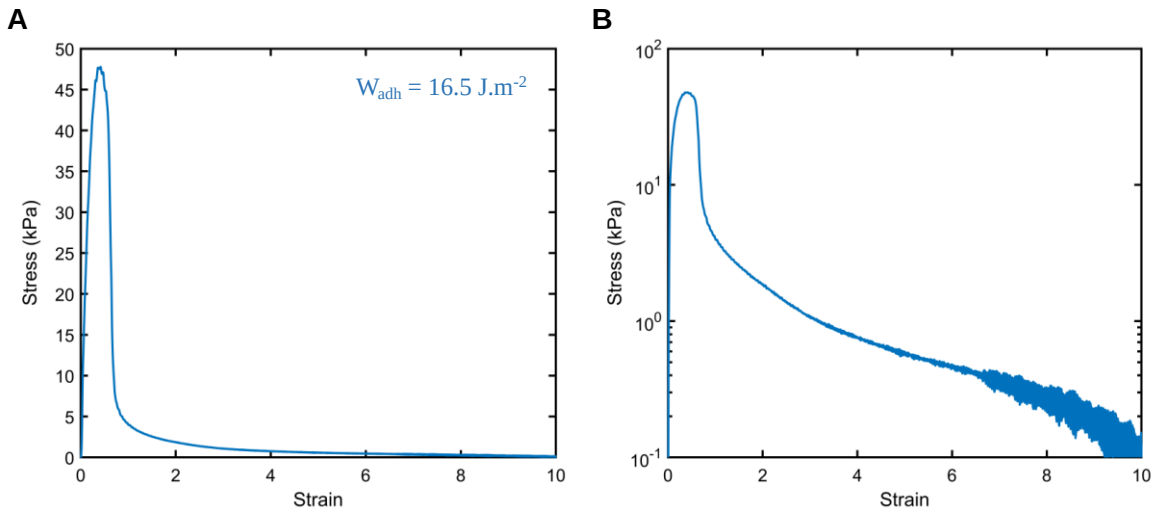

Figure S7. *Nominal stress-strain curves from underwater probe tack experiments on the 0.1 M coacervate after contact with the probes was made directly underwater. The experiment was done at 0.2 s^{-1} after 1 h of immersion.*

Contact time.

Figure S8 A shows the results of probe tack experiments ($\dot{\varepsilon}$ = 0.2 s^{-1}) upon multiple contacts with the 0.1 M coacervate immersed in a 0.1 M NaCl solution. All the tests were carried out after 5 min of contact between the same PAA thin film and adhesive. After detachment, the probe was brought into contact with the adhesive with a total delay of 5 min, roughly corresponding to the total time it took to detach the probe and bring it back into contact (h_0 = 500 µm). As such, C1 represents the first experiment after 5 minutes, while C2 was run after 5 min of contact but 15 min of total immersion in water. Finally, C5 corresponds to a total immersion time of 45 min.

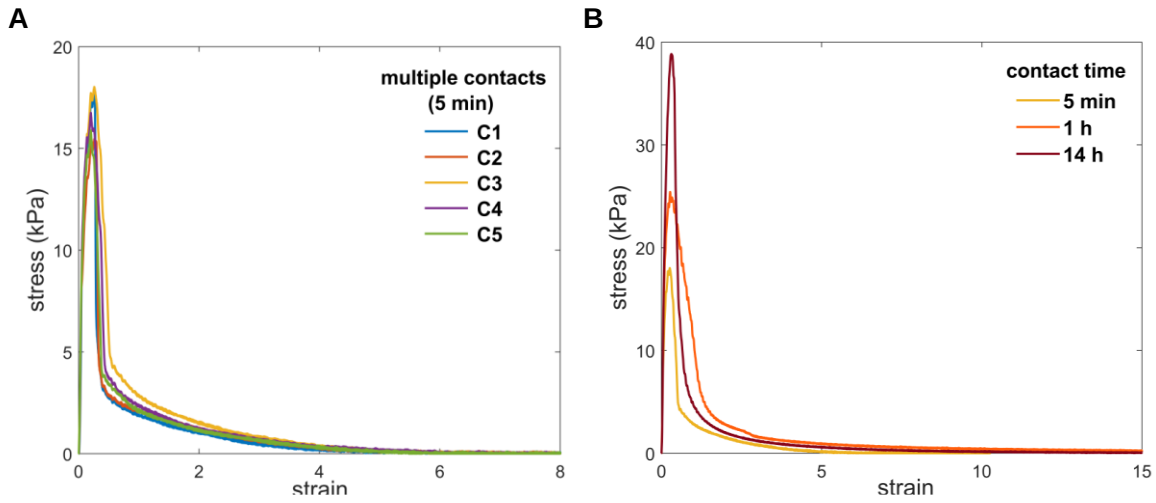

Figure S8. A. *Nominal stress-strain curves from 5 consecutive detachments (C1 − C5) of the probe from the same 0.1 M sample in a 0.1 M NaCl solution (pH = 7), each after 5 min of*

contact. ***B.*** *The effect of contact time on the nominal stress-strain curves from similar probe tack experiments.*

The adhesive behavior of the complex coacervate is characteristic of viscous fluids[8–10] and remains similar among all the contacts. The peak in stress (16.8 ± 1 kPa) drops to a low value where the adhesive is pulled into a fibrillar structure which can be stretched up to strains of 5 – 6. The corresponding adhesion energy averaged for the 5 contacts is 5.0 ± 0.7 $J.m^{-2}$. During these tests, the material was stretched to large deformations, but the eventual failure mode was mostly adhesive with little residue left on the probe.

When the contact between the PAA thin film and the coacervate was allowed to establish for longer time periods (**Figure S8 B**), the material was stretched further ($\varepsilon \approx 15$) and detached cohesively. Despite higher peak stress values for the longest waiting time (14 h), the average adhesion energies do not evolve after 1 h and remain around 13.8 ± 1.9 $J.m^{-2}$ (the W_{adh} corresponding to the experiment after 14 h shown here is 13.5 $J.m^{-2}$). The temporal evolution of the peak stress combined with the change in failure mode (from mainly adhesive to cohesive from 5 min to 1 h or longer) highlight the significance of forming a good interface. This means that longer contact times probably help to establish a stronger interface between the probe and the adhesive. We note that the adhesive itself does not undergo any major switch, as confirmed by linear rheology (see **Figure S6**).

Given that the PAA thin film is charged at pH 7, the strength of the interface relies on both electrostatic interactions and the viscoelasticity of the sample, i.e. its ability to wet the probe. It may be argued that these coacervates are barely charged, with the polycation only 6 mol % in excess. However, charged systems such as complex coacervates and polyampholytes are known for their self-adjustable adhesion against differently-charged surfaces, even when their net charge

is zero.[11–13] The proposed mechanism based on "dynamic ion-bond formation" explains that these materials can adjust their charge on a local level depending on the surface next to which they find themselves, without having to change their net charge. This probably involves configurational changes due to mobility of the charges on the macro-ions along the polymer chain to facilitate the formation of new ion-pairs with the surface; a process which requires time. Cedano-Serrano and coworkers have demonstrated that the underwater adhesion energies of the same PAA thin films against positively charged hydrogels evolve by a factor of 2 between contact times of 1 and 1200 s.[14] We speculate that this dependence is similar or stronger with our complex coacervates.

References

(1) Durand, A.; Hourdet, D. Synthesis and Thermoassociative Properties in Aqueous Solution of Graft Copolymers Containing Poly (N -Isopropylacrylamide) Side Chains. *Polymer (Guildf).* **1999**, *40*, 4941–4951.

(2) Vahdati, M.; Ducouret, G.; Creton, C.; Hourdet, D. Thermally Triggered Injectable Underwater Adhesives. **2020**, *1900653*, 1–7. https://doi.org/10.1002/marc.201900653.

(3) Guo, H.; De Magalhaes Goncalves, M.; Ducouret, G.; Hourdet, D. Cold and Hot Gelling of Alginate-Graft-PNIPAM: A Schizophrenic Behavior Induced by Potassium Salts. *Biomacromolecules* **2018**, *19* (2), 576–587. https://doi.org/10.1021/acs.biomac.7b01667.

(4) Sing, C. E. Development of the Modern Theory of Polymeric Complex Coacervation. *Adv. Colloid Interface Sci.* **2017**, *239*, 2–16. https://doi.org/10.1016/j.cis.2016.04.004.

(5) Cross, M. M. Relation between Viscoelasticity and Shear-Thinning Behaviour in Liquids. *Rheol. Acta* **1979**, *18* (5), 609–614. https://doi.org/10.1007/BF01520357.

(6) Grigorescu, G.; Kulicke, W. M. Prediction of Viscoelastic Properties and Shear Stability of Polymers in Solution. *Adv. Polym. Sci.* **2000**, *152*, 1–40.

(7) Rubinstein, Michael, R. H. C. *Polymr Physics*; Oxford, 2003.

(8) Derks, D.; Lindner, A.; Creton, C.; Bonn, D. Cohesive Failure of Thin Layers of Soft Model Adhesives under Tension. *J. Appl. Phys.* **2003**, *93* (3), 1557–1566. https://doi.org/10.1063/1.1533095.

(9) Nase, J.; Derks, D.; Lindner, A. Dynamic Evolution of Fingering Patterns in a Lifted Hele-Shaw Cell. *Phys. Fluids* **2011**, *23* (12). https://doi.org/10.1063/1.3659140.

(10) Anjos, P. H. A.; Dias, E. O.; Dias, L.; Miranda, J. A. Adhesion Force in Fluids: Effects of Fingering, Wetting, and Viscous Normal Stresses. *Phys. Rev. E - Stat. Nonlinear, Soft Matter Phys.* **2015**, *91* (1), 1–7. https://doi.org/10.1103/PhysRevE.91.013003.

(11) Sun, T. L.; Roy, C. K.; Karobi, S. N.; Ihsan, A. Bin; Kurokawa, T.; Nakajima, T.; Gong, J. P.; Luo, F.; Nonoyama, T. Self-Healing Behaviors of Tough Polyampholyte Hydrogels. *Macromolecules* **2016**, *49* (11), 4245–4252. https://doi.org/10.1021/acs.macromol.6b00437.

(12) Kurokawa, T.; Gong, J. P.; Takahata, M.; Nakajima, T.; Guo, H. L.; Sun, T. L.; Ihsan, A. Bin; Roy, C. K.; Nonoyama, T. Self-Adjustable Adhesion of Polyampholyte Hydrogels. *Adv. Mater.* **2015**, *27* (45), 7344–7348. https://doi.org/10.1002/adma.201504059.

(13) Dompé, M.; Cedano-Serrano, F. J.; Heckert, O.; van den Heuvel, N.; van der Gucht, J.; Tran, Y.; Hourdet, D.; Creton, C.; Kamperman, M. Thermoresponsive Complex Coacervate-Based Underwater Adhesive. *Adv. Mater.* **2019**, *1808179*, 1808179. https://doi.org/10.1002/adma.201808179.

(14) Cedano-Serrano, F. J.; Sidoli, U.; Synytska, A.; Tran, Y.; Hourdet, D.; Creton, C. From Molecular Electrostatic Interactions and Hydrogel Architecture to Macroscopic Underwater Adherence. *Macromolecules* **2019**, *52* (10), 3852–3862. https://doi.org/10.1021/acs.macromol.8b02696.